Simultaneous Estimation of the Time of Disturbance and Inertia in Power Systems

Peter Wall and Vladimir Terzija, *Senior Member, IEEE*

***Abstract*—Offnominal power system frequency regimes play a key role in the propagation of disturbed system conditions and blackouts. The evolution of power systems will make the availability of frequency-control services more uncertain, increasing the risk of large frequency deviations. Furthermore, the reduction in the inherent inertia of power systems and their increased variability will be a critical threat to the quality of frequency control. This paper proposes an online algorithm for estimating the time of disturbance and inertia after a disturbance. This is in contrast to previous inertia estimation methods that operated offline. The algorithm processes wide-area measurements of frequency and active power and could provide support for adaptive frequency control. Simulations, laboratory tests, and real transmission system measurements have been used to demonstrate the algorithm's ability to correctly detect a disturbance, accurately estimate the time of the disturbance and the inertia, and prevent false disturbance detections.**

***Index Terms*—Frequency control, power system disturbances, power system dynamics, power system inertia, smart grids, swing equation, wide-area monitoring systems (WAMS).**

I. Introduction

THE evolution of power systems will threaten the high standard of frequency control that power systems enjoy today. The frequency of a power system is a measure of the balance between generation and load in the system and it changes continuously as the active power flow is never precisely balanced. During normal operation, these changes in frequency are closely controlled by ancillary services that provide continuous, automatic frequency control through automatic generator control (AGC). This includes primary control by generator governors that arrests the change in frequency and secondary control that returns the frequency to approximately nominal [1]. This is necessary due to the high-speed nature of changes in frequency and the need to satisfy stringent power-quality requirements. In the event of a large disturbance, it is important to prevent large deviations of the frequency from the nominal frequency since they can cause the propagation of disturbed system conditions that may lead to cascading failures or even a blackout [2].

Manuscript received September 26, 2013; revised January 12, 2014; accepted February 06, 2014. Date of publication March 06, 2014; date of current version July 21, 2014. This work was supported in part by the EPSRC and in part by the National Grid through the IET Power Networks Research Academy (PNRA). Paper no. TPWRD-01100-2013.

The authors are with the School of Electrical and Electronic Engineering, The University of Manchester, Manchester M13 9PL, U.K. (e-mail: Peter.Wall@manchester.ac.uk; terzija@ieee.org).

Color versions of one or more of the figures in this paper are available online at http://ieeexplore.ieee.org.

Digital Object Identifier 10.1109/TPWRD.2014.2306062

The initial frequency behavior after a disturbance to the active power balance is heavily influenced by system inertia. After a large disturbance (e.g., the loss of a large generator or tie-line), the inertia in the system will influence the depth of the frequency drop and the time available to contain it [3]. Therefore, the system inertia is a critical factor in determining the frequency stability of a power system.

However, the reduction in the number of large synchronous units and their replacement with intermittent generation that is decoupled from the system by power electronics will mean that the inertia in the system will become increasingly variable. In addition to this variability, the inertia will be significantly reduced [4], [5]. These changes will occur at a time when the deployment of Generation III+ nuclear units will increase the size of the largest single credible contingency; for example, the reference incident in the National Grid (U.K. will increase from 1320 to 1800 MW [6]. This is of relevance since the reference incident is used to determine the necessary level of ancillary frequency-control services. Therefore, the power system may be exposed to a larger possible loss of generation and have fewer frequency-control resources.

The ability to determine the system inertia online would help improve situational awareness and offer valuable support for adaptive frequency-control schemes (e.g., adaptive underfrequency load shedding [7]). This support will only be useful if the estimate of the system inertia is performed online and communicated to the relevant operators or controllers quickly enough. Frequency control is expected to operate quickly, with full primary resource deployment within tens of seconds [8] due to the rate at which the frequency can fall after a large disturbance and the risk of the frequency deviation causing secondary disturbances if it is not countered quickly enough.

Therefore, with synchronized measurement technology (SMT), wide-area monitoring systems (WAMS), and other smart-grid infrastructure, further details of which can be found in [9]–[11], will be a necessity for online estimation of the inertia due to the need for a communication infrastructure and measurements of wide-area frequency and active power [12].

Without access to SMT, the existing methods for estimating inertia using the swing equation have been limited to postmortem analysis of frequency measurements recorded during a known disturbance to the system [13]–[15]. It has been shown in [16] that the accuracy of an inertia estimate will be severely undermined by any errors in the estimate of the time of disturbance that is used during the calculation, and the online estimation of this time of disturbance is challenging.

Therefore, creating a method that can accurately and quickly estimate the time of disturbance in the system is vital to realizing

the potential of online inertia estimation. To this end, this paper presents an algorithm for the simultaneous estimation of: 1) the time of disturbance and 2) the inertia of the system at that time. This algorithm is designed to operate online using active power and frequency measurements from a WAMS. The novelty of this algorithm lies in the fact that the simultaneous estimation of the inertia and the time of disturbance means that no additional inputs, beyond the active power and frequency measurements, are necessary to estimate the inertia. This is in contrast to, for example, [13], [14], and [16] where a known time and/or size of disturbance was necessary to perform the inertia estimation.

The algorithm proposed here uses the swing equation, with damping neglected, to model the frequency dynamics of the system immediately after a disturbance. This reduced model is used while the fast-acting nature of frequency control limits the time available for gathering observations of the system response to the disturbance. Therefore, the observations available do not provide sufficient observability of the parameters of more complex models of frequency dynamics to allow their robust estimation.

In its present form, the algorithm processes frequency and active power measurements from a single location. This is suitable in the case of the small systems considered in this paper as the frequency and, consequently, the inertial response of the system can be assumed to be approximately homogenous. However, in larger systems, the frequency and inertial response will vary across the system because frequency waves propagate across the system after a disturbance at speeds of several hundred miles per second [17].

The main body of this paper is structured as follows: Section II gives a brief background to inertia and the swing equation. Section III describes the implementation of the proposed algorithm. Section IV presents some initial results that highlighted a flaw in the method, the solution to which is described in Section V. Further simulation results are then used to analyze the performance of the method in Section VI. Sections VII and VIII present the impact on the performance of the method of changing the number of consecutive samples used to detect a disturbance and the sampling frequency of the data used, respectively. Section IX gives the results of applying the algorithm to data recorded for a motor-generator set in a laboratory and for the National Grid (U.K.) transmission system. Section X discusses the factors that should be considered when selecting the parameter values used by the method. Section XI concludes this paper and suggests some future developments.

II. Theoretical Background

The inertia of a power system is a measure of the stored energy in the rotating masses of the system [18]. The inertia of a rotating shaft is commonly defined using its inertia constant H, which is calculated as follows:

$$H = \frac{J\omega_n^2}{2S_B} \tag{1}$$

where H is the inertia constant in seconds, J is the moment of inertia of the shaft in $\mathrm{kgm^2s}$, S_B is the base power, and ω_n is the nominal speed. Using the nominal speed, instead of the actual speed of the machine, allows H to be defined as a constant. Due to the narrow speed range of power systems, this approximation is acceptable [18]. This stored energy governs the initial frequency response of the power system to a change in the active power according to the swing equation [18]

$$\frac{2H\ df(t)}{dt} = p_m(t) - p_e(t) \tag{2}$$

where p_m is the mechanical power driving the rotor in per unit, p_e is the power across the air gap of the machine in per unit and df/dt is the derivative of frequency in per unit/seconds. The swing (2) can be modified to only contain variables measured on the electrical side of the system by exploiting the slow-changing nature of mechanical power relative to electrical power [18]

$$\frac{2H\ df(t)}{dt} = p_e(t - \Delta t) - p_e(t) \tag{3}$$

where Δt is the interval between measurements and p_e is now the active power at the location at which the derivative of frequency is measured. The validity of this approximation in the context of inertia estimation is demonstrated in [12].

Equation (3) is valid immediately after a disturbance at the location where the frequency and active power measurements are recorded from. Therefore, the algorithm described in this paper will detect the time at which a disturbance is observed at the location being monitored and estimate the inertial response of this location. This renders the selection of the locations that are monitored in the system an important part of the practical application of this algorithm. This issue is not addressed in detail in this paper, since the scope of this paper demonstrates the successful operation of the algorithm. However, some general comments would be that if only a single measurement location is used, then it should represent the general frequency behavior of the system, as in [13] and [14], and if multiple locations are used, they should be spread throughout the system to ensure that each area of the system is properly represented.

III. Time of Disturbance Detection and Power System Inertia Estimation Algorithm

The algorithm presented in this paper is designed to determine the time of a disturbance while simultaneously estimating the inertia at that time. This algorithm is intended to operate online with input data of synchronized measurements of active power and a derivative of frequency that are updated every Δt seconds. The algorithm determines the time of disturbance by detecting the convergence of the output of an inertia estimation algorithm that is based on sliding data windows that continuously process these measurements.

A. Power System Inertia Estimation Algorithm

At the core of this algorithm is a set of four smoothing filters: two for the active power and two for the derivative of frequency, that are applied as sliding data windows to estimate the inertial response of the measured frequency and active power. The windows are labeled P_1, P_2, R_1, and R_2, where P denotes active power and R denotes the derivative of frequency. The subscripts denote the first window and the second window in terms of when they are applied, see Fig. 1.

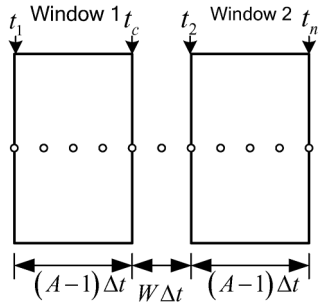

Fig. 1. Pair of windows that are used to process each set of input data. In this example, the black circles are data points so $A = 5$ and $W = 2$.

The windows act as smoothing filters so the estimation process for the time t_n, when a set of new measurements is received, will represent the behavior at time t_c, as depicted in Fig. 1. Each window has a width of A data points and, therefore, a width of $(A-1)\Delta t$ seconds, and the separation between each pair of windows is determined by the width of any prefiltering applied to the data $W\Delta t$ seconds.

For the case where a straight mean of the data points is taken, the output of the windows for the time at which new measurements are received (t_n) can be defined as follows:

$$P_1(t_n) = \frac{1}{A}\sum_{t=t_1}^{t_c} P(t) \tag{4}$$

$$P_2(t_n) = \frac{1}{A}\sum_{t=t_2}^{t_n} P(t) \tag{5}$$

$$R_1(t_n) = \frac{1}{A}\sum_{t=t_1}^{t_c} \dot{f}(t) \tag{6}$$

$$R_2(t_n) = \frac{1}{A}\sum_{t=t_2}^{t_n} \dot{f}(t). \tag{7}$$

Each window provides one of the variables in the swing (3). This can be represented by adjusting the notation of the swing (3) to correspond to the window definitions as follows:

$$H = \frac{0.5(P_1 - P_2)}{(R_2 - R_1)}. \tag{8}$$

This filter design was determined based on the expectation that it must be simple and robust if it is to be feasible for online execution. The windows act as low-pass filters and will help to eliminate the measurement errors that inevitably arise in practice from sources, such as transducers and analog-to-digital conversion.

This direct calculation of H, which is based on four sliding data windows that act as simple and efficient low-pass filters, is used here as the simplicity of the model used renders more complex and unnecessary estimation techniques. This simplicity is of critical importance due to the demands placed on the algorithm in terms of speed and robustness.

The proposed algorithm uses input data of the active power and derivative of frequency measured from a single location, as presented in Fig. 2. The example data in Fig. 2 were generated using the system frequency-response (SFR) model proposed in [19]. The model has an inertia of 5 s and is exposed to a step decrease in load after five seconds. Additive white noise of 0.01 p.u. and 0.001 p.u./s has been added to the active power and derivative of frequency data, respectively.

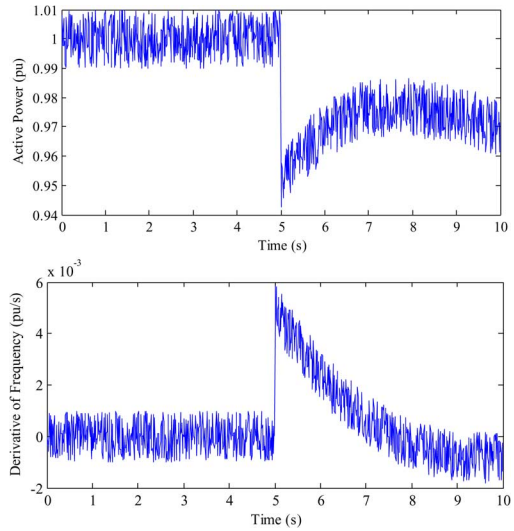

Fig. 2. Algorithm requires measurements of the active power and derivative of frequency. These examples were produced using a MATLAB script of the SFR model proposed in [19] at a sampling rate of 100 Hz.

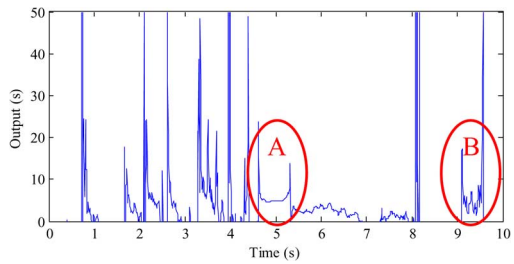

Fig. 3. Output of the windowing process for the example data with a disturbance after 5 s. A and B highlight the behavior of the output for the time of disturbance and for noise.

The output of the proposed algorithm for the signals presented in Fig. 2 is presented in Fig. 3. The time axis in Fig. 3 gives the t_c that the output represents. This is done because it is the t_c for the estimate convergence that will correspond to the time of the disturbance and not t_n. To avoid confusion, the y axis in Fig. 3 is labeled as *Output (s)* because only those estimates for the period of time in which a disturbance has occurred will be estimates of the unknown system inertia, since the model in (2) is only a valid representation of the physical behavior of the system during this time. It can be seen in Fig. 3 that the output converges to approximately the true value of the inertia ($H = 5$ s) during the disturbance. Therefore, with access to this output, the challenge of detecting a disturbance becomes detecting the convergence of the output of the swing equation to an approximately fixed value and estimating the inertia from the observations made during this period of convergence. This can be viewed as a form of feature extraction.

B. Determining the Time of Disturbance

The disturbance detection process presented in this paper exploits the convergent properties of the windowing process

during a disturbance, see Fig. 3. It does this by calculating the residue between $N+1$ consecutive outputs from the windowing process to determine the degree of similarity between them. A new residue is calculated each time a new set of active power and derivative of frequency measurements is received and a disturbance is deemed to have occurred once a certain number of consecutive outputs are sufficiently similar to one another. The current count of sufficiently similar consecutive outputs is defined as the consecutive sum (CSUM). The heuristic nature of this approach allowed a simple and robust algorithm to be created that has performed very well in the examples presented in this paper for simulated and real data.

The benefit of detecting a disturbance based on the convergence of the window output to an approximately constant value is that this convergence is independent of system properties. This is in contrast to detecting the disturbance based on applying thresholds to the behavior of the phase angle, frequency, or active power. These values vary throughout the disturbance and the thresholds must vary with a number of system properties, including the inertia itself, or the size, location, and nature of the disturbance.

A set of $N+1$ consecutive outputs is classqed as being sufficiently similar if the absolute value of the residue between them and the current output is below the *dynamic threshold* r_{MAX}. The residue (r) is calculated as follows, when a new output (H_L) is received at the time t_n

$$r(t_n) = \sum_{t=t_n-N\Delta t}^{t_n-\Delta t} \left(H_L(t) - H_L(t_n)\right)^2. \tag{9}$$

Defined in this way, this residue is the fitting error if the new HL is fitted to the past N H_L values as a straight line with zero gradient. The threshold r_{MAX} is calculated as the product of the current output and a user-defined threshold ratio t_r

$$r_{\mathrm{MAX}}(t_n) = H_L(t_n) tr. \tag{10}$$

The advantage of using this threshold is that it can be defined based on the stochastic properties of the input signals that can be extracted in advance (e.g., the noise in the active power and frequency measurements) and not the properties of the power system. This means that as the system properties (e.g., the inertia) change, the optimum threshold will not, in contrast to a fixed threshold applied to the change in active power or derivative of frequency.

The behavior of CSUM can be described as follows:

$$\mathrm{CSUM}(t_n) = \left(\mathrm{CSUM}(t_n - \Delta t) + 1\right) C_R C_L. \tag{11}$$

CSUM is initialized with a value of zero and then each time a set of consecutive samples satisfies the dynamic threshold, r_{MAX}, CSUM is incremented by one. The binary variable CR is set to one if the residue (r) satisfies r_{MAX} and it is set to zero if it does not; this serves to reset CSUM to zero. The binary variable C_L acts as a form of bad data detection. If the new H_L is less than or equal to zero or greater than or equal to a user-defined limit, H_{MAX}, C_L is set to zero; otherwise, it is one. H_L is limited to H_{MAX} to prevent the algorithm from processing data that is clearly erroneous. In this paper, it is set to ten times the true inertia.

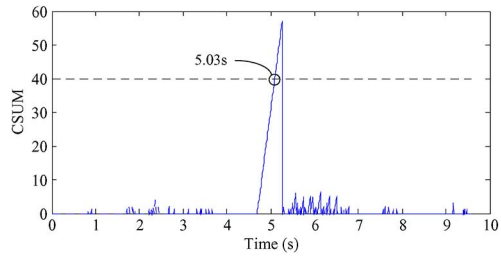

Fig. 4. CSUM is used to determine the presence of a disturbance and it only approaches the detection threshold for the disturbance.

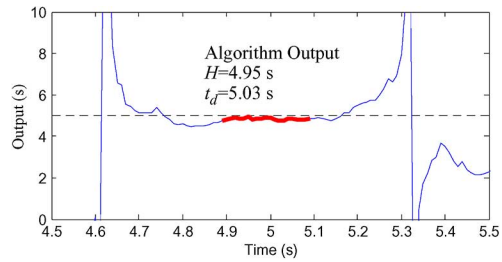

Fig. 5. Example of the targeting process used by the algorithm. This converts the output of the windowing algorithm (blue line) into an inertia estimate using the $A/4$ estimates on either side of td (thick red line).

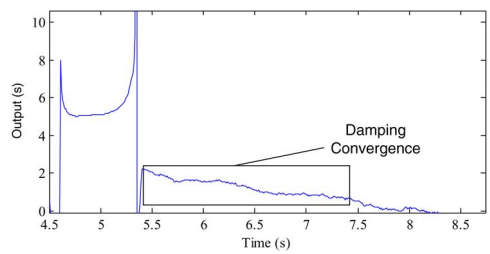

Fig. 6. Postdisturbance oscillations create an extended period of weak convergence that can trigger the algorithm and cause false detection.

Fig. 4 depicts the behavior of CSUM for the example presented in Fig. 3. A disturbance is deemed to have occurred if CSUM is equal to A since there has been convergence for a full window. The time of the disturbance t_d can then be estimated based on the t_n at which CSUM was equal to A by accounting for the delays introduced by each stage

$$t_d = t_n - \left((2A-1) + W\right)\Delta t. \tag{12}$$

Having detected a disturbance and estimated the time of its occurrence, the inertia can be estimated based on the $A/4$ H values on either side of t_d. Fig. 5 shows the result of this process for the example case. The H values that are used from either side of t_d could be varied. This selection must balance the improved robustness offered by taking the mean of multiple estimates against the decline in accuracy of the estimates made for t_c values other than the true time of disturbance t_d.

This algorithm has two key parameters that are defined by the user, namely, A and tr. The other parameters that must be defined by the user are N and H_{MAX}. A suitable value for N is 3, but the results for 5 and 7 are also presented here. H_{MAX}

can be set as an arbitrarily high number that serves to eliminate the unnecessary processing of data that is clearly erroneous. For example, in a power system with inertia that is expected to be in the range between say 4 and 7 s, a value of 50 s for H_{MAX} would be suitable, or the maximum possible inertia of the system could be used, if it is known. Finally, W is determined based on the properties of the measurement system used to obtain the necessary input data. The results presented here study the behavior of the algorithm for values of A and tr, ranging from 10–40 and 0.1–1.5, respectively.

This process can be executed by following these steps:

1) New measurements of derivative of frequency and active power are received at t_n.
2) Calculate a new H value using the windowing process (see Section IIA) and limit it to between zero and H_{MAX}, if H is limited in this way, set C_L to one; else it is zero, and this limited value is H_L.
3) Calculate the total residue between the new H_L value and the N past H_L values (r). See (9).
4) Calculate the dynamic threshold (r_{MAX}) for this new H_L value. See (10).
5) Compare r with r_{MAX} and if it is less than the threshold, set C_R to one; otherwise, set it to zero.
6) Calculate CSUM according to (11).
7) If CSUM is greater than or equal to A, set flag_D to 1.
8) If flag_D has experienced a rising edge, then the time of the disturbance can be calculated using (12).
9) The inertia can then be estimated using the $A/4$ H estimates from either side of t_d.

The output of this process can be demonstrated by continuing the example from Section III-A. Applying the detection algorithm to the window output presented in Fig. 3 using $A = 40$ and $tr = 0.25$ produces the CSUM presented in Fig. 4. The time at which CSUM is equal to A results in a time of disturbance estimate of 5.03 s, and the estimates used to calculate H are shown in Fig. 5. This resulted in an estimate of $H = 4.95$ s, where the true value of inertia was 5.00 s.

IV. Initial Simulated Examples—Test 1

A set of computer-based simulations was performed to investigate the behavior of the algorithm. These simulations used the system frequency response (SFR) model proposed in [19]. The inertia of the model was set to $H = 5$ s. The investigation took the form of varying the parameters A and tr. The algorithm is assessed based on three criteria:

1) security: preventing false detections;
2) reliability: successfully detecting a disturbance;
3) accuracy: accurately estimating the: a) time of the disturbance t_d and b) system inertia H.

The number of consecutive estimates used to calculate the residuals N is set to $N = 3$ for all of the examples presented here. The influence of the value of N is considered in Section VII. The performance of the algorithm is assessed based on the expectation of false detections (an erroneous detection that is not related to the occurrence of a disturbance), true detections (an accurate detection that is related to the occurrence of a disturbance), the error in the inertia estimate, and the time of disturbance estimate. It is assumed that the number of trials is sufficient to allow the expectation to be approximated as a mean.

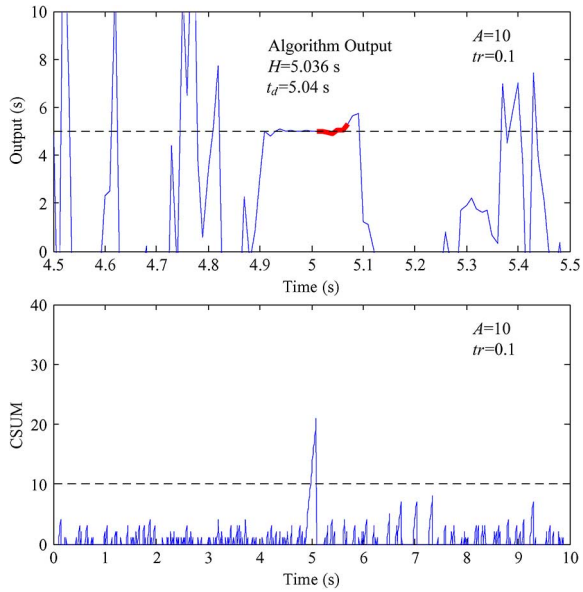

Fig. 7. CSUM and window output for $A = 10$ $tr = 0.1$.

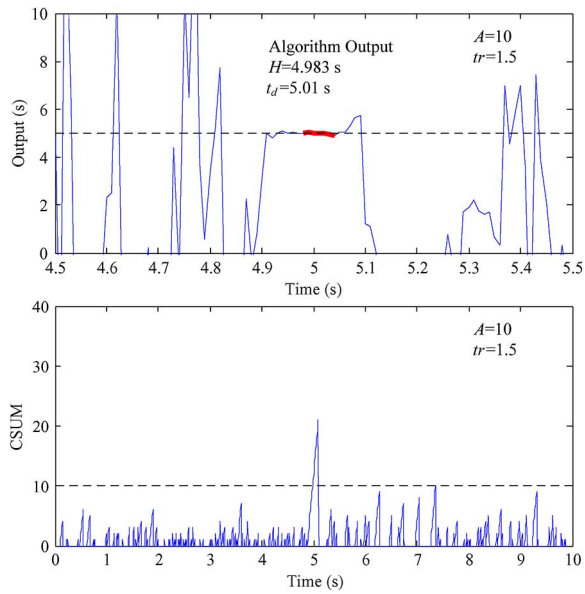

Fig. 8. CSUM and window output for $A = 10$ $tr = 1.5$.

A comparison of the behavior of the output of the windowing process and CSUM for a single example when A values of 10 and 20 and tr values of 0.1 and 1.5 are used can be seen in Figs. 7–10.

Initial results for the expectation of true and false detections, shown in Tables I and II, were generated using 1000 simulations of each A and tr combination with additive white noise of 0.01 p.u. and 0.001 p.u./s for the active power and derivative of frequency measurements, respectively. See Fig. 2 for an example of these signals. Each A and tr combination was exposed to the same 1000 noise signals for consistency. The measurements have a reporting rate of $f_s = 100$ Hz. The disturbance was a 0.2-p.u. step increase in active power demand at $t_d = 5$ s. No

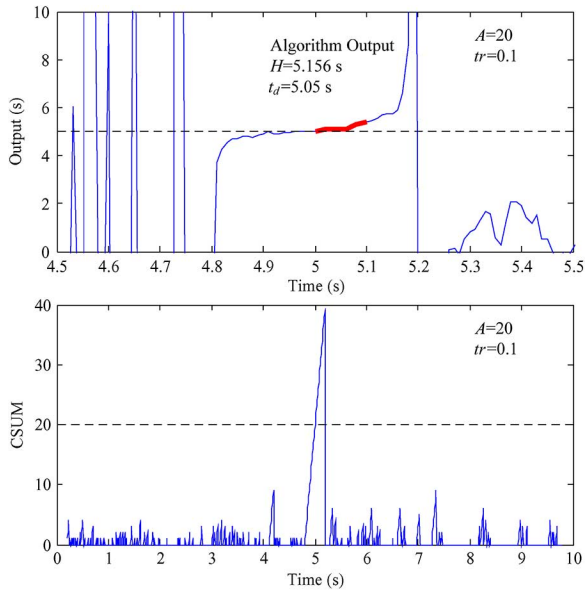

Fig. 9. CSUM and window output for $A = 20$ $tr = 0.1$.

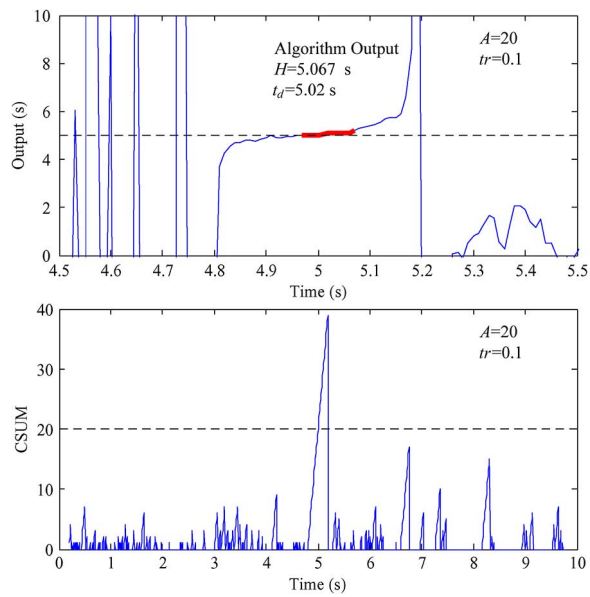

Fig. 10. CSUM and window output for $A = 20$ $tr = 1.5$.

TABLE I
EXPECTATION OF TRUE DETECTIONS FOR TEST 1

tr\A	10	20	30	40
0.1	0.570	0.986	1	1
0.25	1	1	1	1
0.75	1	1	1	1
1.25	1	1	1	1
1.5	1	1	1	1

prefiltering was applied in these simulations since it is not necessary for the success of the algorithm and, thus, serves only to introduce delays. The windowing process with a known time of disturbance is shown to be successful in the presence of prefiltering in [16].

TABLE II
EXPECTATION OF FALSE DETECTIONS FOR TEST 1

tr\A	10	20	30	40
0.1	0	0	0	0
0.25	0	0	0.002	0.130
0.75	0.014	0.504	1.824	1.264
1.25	0.236	2.610	1.684	1.192
1.5	0.618	3.040	1.672	1.212

The results presented in Tables I and II demonstrate that while the algorithm can successfully detect the disturbance, there are a disturbingly high number of false detections. Therefore, the time of disturbance and inertia estimates will not be discussed in this subsection since, in the presence of such a high number of false detections, they are a secondary consideration for the successful development of the algorithm.

The high expectation of false detections exists because of a second convergent period associated with the disturbance, marked in Fig. 6. This convergence is weaker than that seen for the period of the disturbance. As demonstrated by the reduction in false detections that occurs between 20 and 10, that is not accompanied by an equivalent fall in true detections. This occurs because the shorter window offers lower attenuation of the noise so the weaker damping convergence is sufficiently corrupted in order to not always satisfy the convergence threshold, while the stronger true convergence is not.

The number of false detections for $A = 20$, 30, and 40 increases as A is reduced. This occurs because the length of the damping convergence, relative to the window width, makes it possible for the windows to detect the damping convergence multiple times. Since the window width is reduced, this is more likely to occur until the limit is reached at which the window size is too small relative to the noise in the signal.

Possible solutions could include exploiting the influence of tr and A on the false detection rates. However, this is highly undesirable since these parameters are the only tools available to the user to determine the noise tolerance of the algorithm and the size of disturbance that it can reliably detect, and adjusting them to accommodate the issue of damping convergence could severely undermine the performance of the algorithm. Therefore, the solution proposed here is the introduction of a set of *confidence curves* that determine the feasibility of any proposed detection, based on the associated inertia estimate.

V. ELIMINATING FALSE DETECTIONS

This section details the inclusion of a set of limits that will allow the rejection of false detections of the damping convergence. There are two limits: an upperbound (UB) and a lowerbound (LB), which, together, are referred to here as confidence curves and take the form depicted in Fig. 11. Any estimate that lies outside these curves is rejected on the basis that it is extremely unlikely to have actually occurred.

These curves are formed using the following expressions:

$$UB(t) = H_p(1+mv) + (UB_L - H_p(1+mv))\left(1 - 1/1 + \alpha e^{-(t-t_P)\beta}\right) \quad (13)$$

$$LB(t) = H_p(1-mv)$$

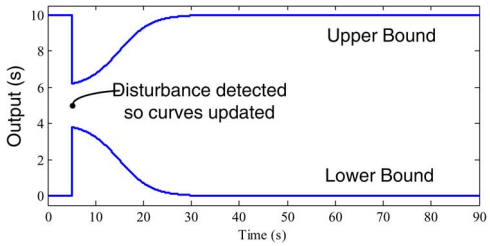

Fig. 11. Confidence curves assess the feasibility of an estimate. Prior to the disturbance, the curves are at the bounds due to a lack of recent information.

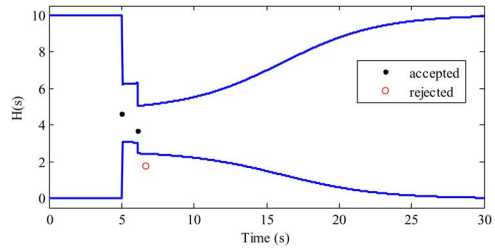

Fig. 12. Confidence curves evolve as the disturbances are detected; the two correct detections are accepted while the false detection is rejected.

$$-\left(LB_L + H_p(1-mv)\right)\left(1 - 1/1 + \alpha e^{-(t-t_P)\beta}\right) \tag{14}$$

where

$$\beta = \frac{-\log(\frac{1}{\alpha})}{0.5\alpha} \tag{15}$$

and H_P and t_P are the value and time of the last known inertia estimate, mv is the maximum expected sudden variation of inertia defined as a proportion of the last known inertia, α is a constant that represents the increase in the likelihood of inertia variation over time by defining the time the curve takes to reach its maximum limit, and UB_L and LB_L are the maximum and minimum values that the inertia is expected to take. The confidence curves use a sigmoidal shape since it is a function that allows a smooth transition between the two limits.

The selection of these parameters must be based on experience with the system in question and those proposed here are suitable for the small simulated model considered in the examples presented in Sections VI–VIII.

The lower bound limit LB_L can be set to zero as the inertia cannot be lower than this so it forms a logical limit. The upper bound limit UB_L can be set to the known maximum inertia (plus some tolerance for error) if one exists. If either of these limits was set to unsuitable values, that is, too high for LB_L or too low for UB_L, then it could allow true detections to be erroneously rejected.

The selection of mv and α should be dictated by the likelihood of variations in the system inertia over time. The value of mv should represent the maximum possible variation in inertia as a percentage of the existing inertia, so a useful value could be the ratio between the largest single loss of inertia possible in the system and the smallest anticipated value of the inertia. The value of α determines the time that it will take the confidence curve to move from the inner limit to the outer limit (e.g., in the case of the upperbound, these are $H_p(1+mv)$ and UB_L, respectively).

The value of mv is likely to be small in most systems, so, in practice, some form of tolerance would have to be added to accommodate the fact that a small difference between two estimates of the inertia could be attributed more to the error of the method than any change in the system. If mv is too small, a second true disturbance would be missed and if it is too large, the confidence curves would cease to work properly.

The selection of α should indicate the confidence that the operator has in the limit imposed by mv continuing to be valid as time passes. If α is too large, then true detections in the future could be incorrectly rejected on the basis that the inertia estimate is outside the curves. If alpha is too small, then mv would not be enforced properly and false detections could occur. It is likely that if the practical application of these curves was to be considered that the selection of mv and α would require detailed knowledge of the system and its operating practices.

TABLE III
DETECTIONS MADE FOR CONFIDENCE CURVES EXAMPLE

Detection	t_d	$H_{estimated}$	H_{true}
1 – accepted	5.04	4.64	4.50
2 – accepted	6.11	3.69	3.50
3 – rejected	6.68	1.75	3.50

The functionality of these curves can be demonstrated by using a simple example in which the SFR model is used to simulate the cascade loss of two large generating units. The first generation loss occurs at 5 s and is a 0.2-p.u. drop in power and a 0.5-s drop in inertia. The second generation loss occurs at 6 s and is a 0.2-p.u. drop in power and a 1-s drop in inertia. The noise magnitudes are 0.01 p.u. for active power and 0.001 p.u./s for the derivative frequency.

Applying the algorithm with $A = 40$ and $tr = 0.25$ to this scenario resulted in three event detections—the first two were accurate detections of the disturbances and the third was a false detection triggered by the damping behavior. These detections are presented in Table III alongside the decision made based on the confidence curves. Fig. 12 shows the evolution of the confidence curves as the events are detected. The settings for these curves are $mv = 0.3$, $\alpha = 30$, $UB_L = 10$, and $LB_L = 0$. This example also serves to demonstrate the ability of the algorithm to detect a second disturbance during the postdisturbance oscillation of the first disturbance.

VI. FURTHER SIMULATED EXAMPLES

A. Repeating Test 1 With Confidence Curves—Test 2

The simulations performed here use the same approach as used in Section IV. The SFR model is simulated using inertia of 5 s and measurements are recorded at a rate of 100 Hz. The algorithm uses three consecutive estimates to calculate the residuals ($N = 3$) and the confidence curves presented in Section V are included in the algorithm. The curves are defined using: $mv = 0.3, \alpha = 30, UB_L = 10, LB_L = 0$. This test involved a 0.2-p.u. load increase after 5 s with additive white noise of 0.01 p.u. for the power and 0.001 p.u./s for the derivative of frequency.

TABLE IV
EXPECTATION OF TRUE DETECTIONS FOR TEST 2

tr\A	10	20	30	40
0.1	0.569	0.986	1	1
0.25	1	1	1	1
0.75	1	1	1	1
1.25	1	1	1	1
1.5	1	1	1	1

TABLE V
EXPECTATION OF FALSE DETECTIONS FOR TEST 2

tr\A	10	20	30	40
0.1	0	0	0	0
0.25	0	0	0	0
0.75	0.012	0.004	0	0
1.25	0.06	0.032	0	0
1.5	0.175	0.038	0	0

TABLE VI
EXPECTATION OF ERROR IN INERTIA ESTIMATE (%) FOR TEST 2

tr\A	10	20	30	40
0.1	-0.355	-1.281	-1.922	-2.303
0.25	-0.159	-0.971	-1.637	-2.089
0.75	-0.076	-0.888	-1.554	-1.998
1.25	0.061	-0.818	-1.511	-1.930
1.5	0.303	-0.783	-1.472	-1.902

TABLE VII
EXPECTATION OF THE ESTIMATED TIME OF DISTURBANCE (S) FOR TEST 2

tr\A	10	20	30	40
0.1	5.04	5.06	5.06	5.06
0.25	5.03	5.04	5.04	5.04
0.75	5.03	5.03	5.03	5.03
1.25	5.02	5.02	5.02	5.02
1.5	5.02	5.02	5.02	5.01

The results of this test are given in Tables IV–VII. These results show that the confidence curves have practically eliminated the false detections seen in Test 1 without compromising the true detections. Furthermore, the accuracy of the time of disturbance and inertia estimates is very good.

B. Investigating the Effects of Increasing the Noise in the Input Signals—Test 3

The proposed method uses the convergence of the output of the windowing process (8) to determine if a disturbance has occurred. This decision is made based on the evaluation of (10) and (11), and the user-controlled variable tr is used to define the tolerance for variations in the output. This process allows the threshold to be defined in terms of the noise in the input signals to the windowing process. Therefore, it is necessary to investigate the influence of changes in this noise on the performance of the method. To this end, Test 2 is repeated here as Test 3 with the noise level used increased by a factor of 5 to 0.05 p.u. for the power and 0.005 p.u./s for the derivative of frequency. The results for Test 3 are presented in Tables VIII–XI.

TABLE VIII
EXPECTATION OF TRUE DETECTIONS FOR TEST 3

tr\A	10	20	30	40
0.1	0	0	0	0.015
0.25	0.050	0.418	0.860	0.983
0.75	0.945	1	1	1
1.25	0.998	1	1	1
1.5	0.999	1	1	1

TABLE IX
EXPECTATION OF FALSE DETECTIONS FOR TEST 3

tr\A	10	20	30	40
0.1	0	0	0	0
0.25	0	0	0	0
0.75	0	0	0	0
1.25	0.005	0.001	0	0
1.5	0.014	0.009	0	0

TABLE X
EXPECTATION OF ERROR IN INERTIA ESTIMATE (%) FOR TEST 3

tr\A	10	20	30	40
0.1	-	-	-	-5.142
0.25	0.173	-1.917	-2.324	-3.188
0.75	-1.042	-1.206	-1.222	-2.074
1.25	-0.545	-1.122	-1.099	-1.962
1.5	-0.501	-1.139	-1.067	-1.926

TABLE XI
EXPECTATION OF THE ESTIMATED TIME OF DISTURBANCE (S) FOR TEST 3

tr\A	10	20	30	40
0.1	-	-	-	5.18
0.25	5.05	5.08	5.10	5.11
0.75	5.04	5.04	5.04	5.05
1.25	5.03	5.03	5.03	5.03
1.5	5.02	5.03	5.03	5.03

These results indicate, unsurprisingly, that as the noise level increases, the expectation of a true detection falls significantly for the lower values of tr that are studied here. This occurs because the increased noise level corrupts the convergent period during the disturbance, particularly in the case of the lowest A value. This also leads to a reduction in the expectation of false detections.

The increased noise level has also caused an increase in the tendency toward the estimate of the time of disturbance being late (i.e., the estimated time is after the true time). This is because the earlier outputs of the windowing process during the disturbance are less convergent and, hence, more vulnerable to the noise, which delays the detection of the convergence. This behavior is responsible for the increase in the tendency of the algorithm to overestimate the inertia because, in general, the convergent period has a small positive gradient, instead of the ideal case of zero gradient, which causes the later outputs of the windowing process during the convergent period to be greater than the true value.

TABLE XII
EXPECTATION OF TRUE DETECTIONS FOR TEST 4

tr\A	10	20	30	40
0.1	0	0	0.021	0.115
0.25	0.149	0.740	0.973	0.999
0.75	0.982	1	1	1
1.25	0.999	1	1	1
1.5	0.997	0.999	1	1

TABLE XIII
EXPECTATION OF FALSE DETECTIONS FOR TEST 4

tr\A	10	20	30	40
0.1	0	0	0	0
0.25	0	0	0	0
0.75	0	0	0	0
1.25	0.006	0.008	0.006	0.006
1.5	0.02	0.022	0.025	0.012

TABLE XIV
EXPECTATION OF ERROR IN INERTIA ESTIMATE (%) FOR TEST 4

tr\A	10	20	30	40
0.1	-	-	-1.131	-5.307
0.25	-1.231	-2.066	-2.321	-2.881
0.75	-1.027	-1.214	-1.568	-2.046
1.25	-1.000	-1.156	-1.508	-1.950
1.5	-1.018	-1.175	-1.481	-1.927

TABLE XV
EXPECTATION OF THE ESTIMATED TIME OF DISTURBANCE (S) FOR TEST 4

tr\A	10	20	30	40
0.1	-	-	5.13	5.16
0.25	5.05	5.08	5.09	5.09
0.75	5.03	5.04	5.04	5.04
1.25	5.02	5.03	5.03	5.03
1.5	5.02	5.02	5.02	5.03

TABLE XVI
EXPECTATION OF TRUE DETECTIONS FOR TEST 5

tr\A	10	20	30	40
0.1	0	0	0	0
0.25	0	0	0	0
0.75	0.014	0.086	0.360	0.690
1.25	0.149	0.588	0.928	0.994
1.5	0.259	0.802	0.980	0.998

TABLE XVII
EXPECTATION OF FALSE DETECTIONS FOR TEST 5

tr\A	10	20	30	40
0.1	0	0	0	0
0.25	0	0	0	0
0.75	0	0	0	0
1.25	0.002	0	0	0
1.5	0.012	0	0	0

TABLE XVIII
EXPECTATION OF ERROR IN INERTIA ESTIMATE (%) FOR TEST 5

tr\A	10	20	30	40
0.1	-	-	-	-
0.25	-	-	-	-
0.75	25.168	-9.900	-6.123	-5.350
1.25	51.118	-2.123	-3.950	-3.159
1.5	53.509	-2.075	-3.558	-2.734

TABLE XIX
EXPECTATION OF THE ESTIMATED TIME OF DISTURBANCE (S) FOR TEST 5

tr\A	10	20	30	40
0.1	-	-	-	-
0.25	-	-	-	-
0.75	5.06	5.09	5.12	5.14
1.25	5.04	5.08	5.10	5.11
1.5	5.04	5.07	5.08	5.09

C. Investigating the Effects of Reducing the Size of the Disturbance—Tests 4 and 5

The disturbance size is now reduced from 0.2 to 0.05 p.u. and Tests 2 and 3 are repeated, as Tests 4 and 5, respectively. This is done to investigate the behavior of the algorithm for a smaller disturbance. The results for these tests are given in Tables XII–XIX. The table entries marked with a dash denote those settings that returned no estimates. The number of false detections has fallen due to the smaller disturbance size limiting the damping convergence.

The accuracy of the estimates is generally good but it has been reduced somewhat when compared to Tests 2 and 3. However, the shortest window width of 10 does not follow this trend. While it was capable of accurately detecting the time of the disturbance, although with a drastically reduced expectation, it could not accurately estimate H due to the noise in the signals. As before, the tendency is toward an overestimate of H and increasing tr limits this but increasing A aggravates it.

VII. VARYING THE NUMBER OF CONSECUTIVE SAMPLES (N) USED TO TEST FOR CONVERGENCE

This section presents the repetition of Test 2 from the previous section for N values of 5 (Test 6) and 7 (Test 5), where N is the number of consecutive samples that are used to calculate the residue r and test for convergence. For this purpose, the residue calculation given in (9) is modified into the form given below

$$r(t_n) = \frac{3}{N} \sum_{t=t_n-N\Delta t}^{t_n-\Delta t} \left(H_L(t) - H_L(t_n)\right)^2 . \qquad (16)$$

This scales the calculated residue according to the value of N used, relative to the value of 3 used in the previous tests so that there is consistency between the tr values in each test case. The results for these tests are presented in Tables XX–XXIII for Test 6, where $N = 5$, and Tables XXIV–XXVII for Test 7, where $N = 7$.

A comparison of these results to those seen for Test 2 ($N = 3$) reveals that as N is increased, the measures used to assess

TABLE XX
EXPECTATION OF TRUE DETECTIONS FOR TEST 6 ($N = 5$)

tr\A	10	20	30	40
0.1	0.332	0.932	0.996	1
0.25	0.987	1	1	1
0.75	1	1	1	1
1.25	1	1	1	1
1.5	1	1	1	1

TABLE XXI
EXPECTATION OF FALSE DETECTIONS FOR TEST 6 ($N = 5$)

tr\A	10	20	30	40
0.1	0	0	0	0
0.25	0	0	0	0
0.75	0	0	0	0
1.25	0.01	0	0	0
1.5	0.038	0.004	0	0

TABLE XXII
EXPECTATION OF ERROR IN INERTIA ESTIMATE (%) FOR TEST 6 ($N = 5$)

tr\A	10	20	30	40
0.1	-1.472	-1.712	-1.978	-2.529
0.25	-1.213	-1.340	-1.654	-2.235
0.75	-0.942	-1.175	-1.521	-2.099
1.25	-0.700	-1.078	-1.438	-2.024
1.5	-0.617	-1.028	-1.399	-1.979

TABLE XXIII
EXPECTATION OF THE ESTIMATED TIME OF DISTURBANCE (S) FOR TEST 6 ($N = 5$)

tr\A	10	20	30	40
0.1	5.06	5.07	5.08	5.08
0.25	5.05	5.05	5.05	5.05
0.75	5.04	5.04	5.04	5.04
1.25	5.03	5.03	5.03	5.03
1.5	5.02	5.02	5.02	5.02

TABLE XXIV
EXPECTATION OF TRUE DETECTIONS FOR TEST 7 ($N = 7$)

tr\A	10	20	30	40
0.1	0.158	0.794	0.940	0.997
0.25	0.856	1	1	1
0.75	1	1	1	1
1.25	1	1	1	1
1.5	1	1	1	1

TABLE XXV
EXPECTATION OF FALSE DETECTIONS FOR TEST 7 ($N = 7$)

tr\A	10	20	30	40
0.1	0	0	0	0
0.25	0	0	0	0
0.75	0	0	0	0
1.25	0.007	0.001	0	0
1.5	0.029	0.004	0	0

TABLE XXVI
EXPECTATION OF ERROR IN INERTIA ESTIMATE (%) FOR TEST 7 ($N = 7$)

tr\A	10	20	30	40
0.1	-1.721	-1.974	-2.387	-2.870
0.25	-1.755	-1.636	-1.939	-2.482
0.75	-1.193	-1.353	-1.738	-2.290
1.25	-0.913	-1.208	-1.607	-2.168
1.5	-0.839	-1.136	-1.552	-2.107

TABLE XXVII
EXPECTATION OF THE ESTIMATED TIME OF DISTURBANCE (S) FOR TEST 7 ($N = 7$)

tr\A	10	20	30	40
0.1	5.07	5.09	5.09	5.10
0.25	5.07	5.07	5.07	5.07
0.75	5.05	5.05	5.05	5.05
1.25	5.03	5.03	5.04	5.04
1.5	5.03	5.03	5.03	5.03

the method follow the same trends as seen in Test 2 for a decrease in tr. Namely, that as N increases, the overestimation of H increases, the lateness of the time of disturbance estimate increases, the likelihood of a true detection falls, and the likelihood of false detections falls. This behavior is driven by the fact that increasing N increases the likelihood that a set of consecutive samples will be rejected by the convergence threshold as more samples are tested and, consequently, the likelihood of both true and false detections will fall.

This increased likelihood of rejection is particularly true for those consecutive samples found earlier in the convergent period, since they are less convergent (see Figs. 7–10), which drives the increase in the lateness of the time of disturbance detection. This increase causes a consequent increase in the overestimation of H because the train of output values during the disturbance, while ideally a straight line with a gradient of zero, tends to have a positive gradient. This positive gradient is most likely caused by the increasing influence of factors, other than the inertia, on the frequency that are not accounted for in the swing (8) used to calculate the candidate H estimates.

VIII. VARYING THE SAMPLING FREQUENCY OF THE INPUT MEASUREMENTS

This section presents the results of repeating Test 2 with $N = 3$ and for input measurements with two different sampling frequencies; these are 50 Hz (Test 8) and 25 Hz (Test 9). Previously, the width of the filter windows A has been defined in terms of the number of data points they cover. For these tests, the A values used for the different sampling rates are selected so that they cover the same, or approximately the same, amount of time in seconds as those selected in Test 2.

These results are presented in Tables XXVIII–XXXV. It can be seen that as the sampling frequency of the input data is reduced, the likelihood of true detections falls for the lower A and tr values. This occurs because the data points within the convergent period are further apart in terms of time; therefore, they are less similar so the residues between them will be larger, and without a compensating increase in tr, this will reduce the likelihood of true detection. In contrast, the number of false detections increases as the sampling frequency falls. This is because the convergence threshold is smaller in terms of data points;

TABLE XXVIII
EXPECTATION OF TRUE DETECTIONS FOR TEST 8 (50 Hz)

tr\A	5	10	15	20
0.1	0.099	0.533	0.815	0.927
0.25	0.742	1	1	1
0.75	1	1	1	1
1.25	0.990	1	1	1
1.5	0.974	1	1	1

TABLE XXIX
EXPECTATION OF FALSE DETECTIONS FOR TEST 8 (50 Hz)

tr\A	5	10	15	20
0.1	0	0	0	0
0.25	0	0	0	0
0.75	0.001	0	0	0
1.25	0.045	0	0	0
1.5	0.1	0.007	0	0

TABLE XXX
EXPECTATION OF ERROR IN INERTIA ESTIMATE (%) FOR TEST 8 (50 Hz)

tr\A	5	10	15	20
0.1	-0.075	-2.049	-2.737	-3.285
0.25	-0.417	-1.753	-2.050	-2.567
0.75	-0.246	-1.491	-1.856	-2.371
1.25	0.074	-1.273	-1.750	-2.248
1.5	0.109	-1.129	-1.699	-2.178

TABLE XXXI
EXPECTATION OF THE ESTIMATED TIME OF DISTURBANCE (S) FOR TEST 8 (50 Hz)

tr\A	5	10	15	20
0.1	5.06	5.09	5.10	5.11
0.25	5.06	5.07	5.07	5.07
0.75	5.05	5.05	5.05	5.05
1.25	5.03	5.03	5.04	5.03
1.5	5.03	5.03	5.03	5.03

TABLE XXXII
EXPECTATION OF TRUE DETECTIONS FOR TEST 9 (25 Hz)

tr\A	3	5	8	10
0.1	0.004	0.094	0.240	0.261
0.25	0.056	0.680	0.958	0.996
0.75	0.339	0.999	1	1
1.25	0.832	0.993	1	1
1.5	0.815	0.988	1	1

TABLE XXXIII
EXPECTATION OF FALSE DETECTIONS FOR TEST 9 (25 Hz)

tr\A	3	5	8	10
0.1	0	0	0	0
0.25	0.001	0	0	0
0.75	0.054	0.001	0	0
1.25	0.206	0.010	0.002	0
1.5	0.325	0.026	0.004	0

TABLE XXXIV
EXPECTATION OF ERROR IN INERTIA ESTIMATE (%) FOR TEST 9 (25 Hz)

tr\A	3	5	8	10
0.1	3.437	-1.484	-4.131	-3.999
0.25	6.187	-1.525	-3.314	-3.690
0.75	-0.407	-1.369	-2.742	-3.102
1.25	-1.275	-0.659	-2.282	-2.639
1.5	-1.270	-0.652	-2.156	-2.535

TABLE XXXV
EXPECTATION OF THE ESTIMATED TIME OF DISTURBANCE (S) FOR TEST 9 (25 Hz)

tr\A	3	5	8	10
0.1	5.09	5.12	5.15	5.15
0.25	5.09	5.12	5.13	5.13
0.75	5.07	5.10	5.10	5.10
1.25	5.05	5.07	5.07	5.07
1.5	5.05	5.06	5.06	5.06

therefore, it is more likely that a false convergent period will occur.

A reduction in sampling frequency also aggravates the tendency of the method to generate a late estimate of the true disturbance time, that is, the estimated time is after the true time. For the larger A values, this causes a corresponding increase in the tendency to overestimate the inertia due to the positive gradient of the output during the true convergent period. This trend is not seen for the lower A values as, in many cases, the low number of true detections, combined with the small number of data points used to calculate the mean value of the inertia, means that the mean of the estimate errors is vulnerable to being skewed by a small number of outliers.

IX. LABORATORY AND FIELD DATA TESTS

A. Laboratory-Based Motor-Generator Set

The algorithm was applied to measurements from the laboratory testing of a motor-generator (MG) set. Two separate tests were performed: the first of these was a load increase of 75 W at 3.42 s and the second was a load increase of 300 W at 1.69 s. The active power and the derivative of frequency of the MG set are shown in Fig. 13 and details of the laboratory setup are given in [20]. The proposed algorithm was applied to these measurements using $A = 20$ and $tr = 0.75$. The data were prefiltered with a width of 6 samples, so $W = 6$. The results of the algorithm are presented in Figs. 14 and 15. The time of disturbance estimates of 3.48 and 1.68 represent an error of 0.06 and 0.01 s, respectively. The H estimates of 4.76 and 4.81 s are consistent, and there are no false detections so it was unnecessary to consider the settings for the confidence curves.

B. Real-life National Grid (U.K.) Example

The algorithm was applied to data recorded by the National Grid (U.K.). On May 27, 2008, the system experienced the sequential loss of two generating units—Longannet (345 MW) and Sizewell B (1237 MW). The frequency during these disturbances is given in Fig. 16, and the sampling frequency of the measurements is $f_s = 25$ Hz. The results of applying the algorithm with $A = 45$ and $tr = 1.75$ are presented in Figs. 17 and

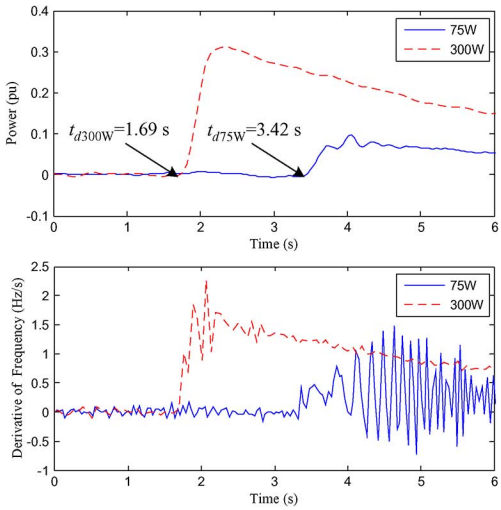

Fig. 13. Data recorded for two load changes applied to a motor-generator set that is used to test the algorithm.

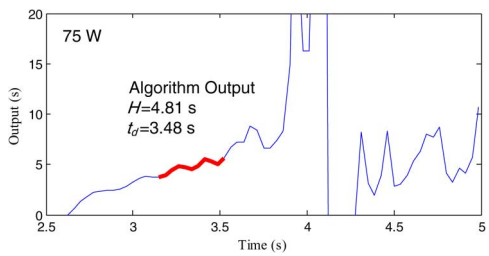

Fig. 14. Algorithm output for a 75-W step increase in the MG set load. The bold red line marks the values used to estimate H.

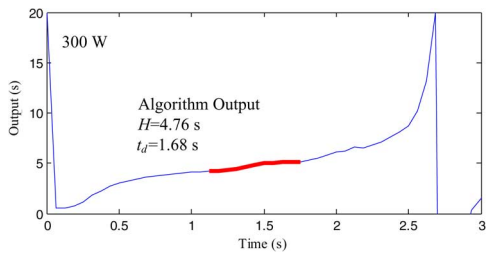

Fig. 15. Algorithm output for a 300-W step increase in the MG set load. The bold red line marks the values used to estimate H.

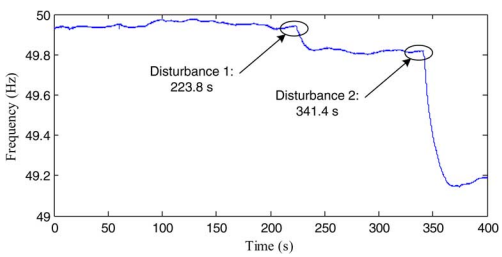

Fig. 16. Frequency during the disturbances seen in the National Grid.

18. The time of disturbance estimates of 224.0 and 341.7 s represent errors of 0.2 and 0.3 s, respectively. The inertia estimates of 8.87 and 9.33 s are on a base of 43 000 MW, which was selected since it is the approximate load of the system at the time of the disturbances. A more natural base would be the rating of

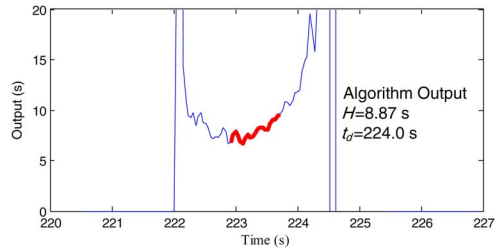

Fig. 17. Algorithm output for the first disturbance in the national grid example, loss of Longannet (345 MW) after 223.8 s. The bold red line marks the values used to estimate H.

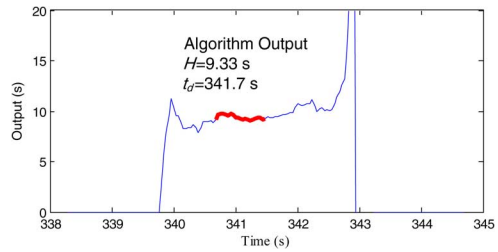

Fig. 18. Algorithm output for the second disturbance in the national grid example, loss of Sizewell B (1237 MW) after 341.4 s. The bold red line marks the values used to estimate H.

the generators in service but this information was unavailable. These estimates are reasonably consistent and there are no false detections so it was unnecessary to consider the settings for the confidence curves.

X. Selecting Parameter Values

The proposed method has a number of parameters that must be selected properly if it is to offer a suitable level of performance. However, it is the proper selection of A and tr that is most integral to the proper behavior of the proposed method.

The range of values used in the simulations presented here is intended to describe the behavior of the method as A and tr vary and are not proposed as a correct set of values in general. In practice, it is likely that the selection of suitable values of A and tr will require some form of supervised training process that can tailor the selection of A and tr, and the other method parameters (e.g., mv and α) to the system and input signals. This process will be influenced by the power system, which will determine the nature of the confidence curves, and the properties of the measurement system (e.g., the sampling frequency and the statistical properties of the noise), which will influence A, tr, and N.

However, the results presented in Sections VI–VIII do indicate that for a given noise level and sampling frequency, a range of suitable A, N, and tr combinations do exist.

Several factors must be considered when selecting A and tr. The most noticeable of these is that tr must be increased as the noise increases to ensure that the disturbance is detected. An increase in tr also allows smaller disturbances to be detected.

Increasing tr causes fewer of the earlier estimates in the convergent period to be discarded as nonconvergent so the time of disturbance estimate is more accurate. Including these earlier

estimates also limits the tendency of the algorithm to overestimate H. However, increasing tr also increases the risk of false detections so a balance must be struck.

The main advantage of increasing A is that it serves to reduce the risk of false detections and increase the likelihood of true detections. However, increasing A increases the degree to which H and the time of disturbance will be overestimated and introduces additional delays into the algorithm.

While the selection of N does influence the algorithm performance, it is less significant than other factors, such as A, tr, the statistical properties of the anticipated noise level, and the sampling frequency. Therefore, when considering parameter selection for the proposed method, it may be possible to reduce the complexity of the problem by fixing N to a single value.

Finally, the sampling frequency of the input signals has a significant influence on the suitable values of A and tr. The results in Section VIII suggest that for lower sampling frequencies, a larger A value, in terms of the time the windows cover, should be used. Furthermore, tr should also be increased to accommodate the greater time difference between adjacent points.

XI. Conclusions

This paper presented a new approach for simultaneously performing the online estimation of the time of a disturbance in a power system and the inertia of the system immediately after the disturbance. This algorithm uses a set of sliding data windows to continuously calculate candidate inertia estimates. These candidate estimates will converge to the true inertia during a disturbance. The residues between these candidate estimates are used to detect this convergence and consequently detect the disturbance and estimate the time at which it occurred. The output of the windows during this period can then be used to estimate the inertia in the system.

The results presented in Sections IV–IX demonstrate that the proposed algorithm can accurately estimate the time of disturbance and inertia for both small and large disturbances as well as for both simulated data and data recorded from the field when suitable parameter values are used. The results presented demonstrate that the algorithm parameters (A and tr) must be selected based on experience with the system, the expected noise level, and the size of disturbance that the algorithm is expected to detect. This method could be improved by introducing a control loop that automatically adjusts the algorithm parameters (most likely tr) as the noise conditions in the system change. It could also be possible to use the duration of the convergent period (the time for which $flag_D$ is high) as a measure of the certainty that a disturbance has occurred. Furthermore, the potential risk of convergence to an erroneous value of H for higher noise levels and smaller window sizes that can be observed in Test 3 may require further investigation.

The issues related to applying the method to larger power systems in which the frequency behavior of the system varies spatially should also be a topic of further work. This will involve the analysis of how to incorporate measurements from multiple locations into a single method that, rather than returning a single estimate of inertia, returns some form of inertia fingerprint for the system that would allow the spatial variation in the frequency response and inertia to be observed online.

Finally, if practical implementation of this method was to be considered, it would be attractive to develop a recursive form due to the large quantity of data buffering that is necessary in its existing nonrecursive form.

References

[1] J. Machowski, J. W. Bialek, and J. R. Bumby, *Power System Dynamics: Stability and Control*, 2nd ed. Chichester, U.K.: Wiley, 2008.

[2] U. S.-Canada Power System Outage Task Force, Final report on the August 14, 2003 blackout in the United States and Canada: Causes and recommendations, 2013. [Online]. Available: http://www.nerc.com/comm/PC/System%20Protection%20and%20Control%20Subcommittee%20SPCS%20DL/Full_Final_Report.pdf

[3] P. Kundur, N. J. Balu, and M. G. Lauby, *Power System Stability and Control*. New York: McGraw-Hill, 1994.

[4] R. J. Best, C. F. Ten, D. J. Morrow, and P. A. Crossley, "Synchronous island control with significant contribution from wind power generation," presented at the CIGRE/IEEE Power Energy Soc. Joint Symp. Integr. Wide-Scale Renew. Resources Into Power Del. Syst., Calgary, AB, Canada, Jul. 2009.

[5] A. Mullane, G. Bryans, and M. O'Malley, "Kinetic energy and frequency response comparison for renewable generation systems," presented at the Int. Conf. Future Power Syst., Amsterdam, the Netherlands, Nov. 18, 2005.

[6] National Grid, "Electricity ten year statement," Warwick, U.K., 2013. [Online]. Available: https://www.nationalgrid.com/uk/Electricity/ten-year-statement/

[7] V. Terzija, "Adaptive underfrequency load shedding based on the magnitude of the disturbance estimation," *IEEE Trans. Power Syst.*, vol. 21, no. 3, pp. 1260–1266, Aug. 2006.

[8] Y. G. Rebours, D. S. Kirschen, M. Trotignon, and S. Rossignol, "A survey of frequency and voltage control ancillary services—Part I: Technical features," *IEEE Trans. Power Syst.*, vol. 22, no. 1, pp. 350–357, 357, Feb. 2007.

[9] A. G. Phadke and J. S. Thorp, *Synchronized Phasor Measurements and their Applications*. New York: Springer, 2008.

[10] V. Terzija, G. Valverde, D. Cai, P. Regulski, V. Madani, J. Fitch, S. Skok, M. M. Begovic, and A. Phadke, "Wide-area monitoring, protection, control of future electric power networks," *Proc. IEEE*, vol. 99, no. 1, pp. 80, 93, Jan. 2011.

[11] S. Chakrabarti, E. Kyriakides, B. Tianshu, D. Cai, and V. Terzija, "Measurements get together," *IEEE Power Energy Mag.*, vol. 7, no. 1, pp. 41–49, Jan./Feb. 2009.

[12] P. Wall, F. González-Longatt, and V. Terzija, "Demonstration of an inertia constant estimation method through simulation," in *Proc. 45th Int. Univ. Power Eng. Conf.*, Aug. 31–Sep. 3, 2010, pp. 1, 6.

[13] T. Inoue, H. Taniguchi, Y. Ikeguchi, and K. Yoshida, "Estimation of power system inertia constant and capacity of spinning-reserve support generators using measured frequency transients," *IEEE Trans. Power Syst.*, vol. 12, no. 1, pp. 136–143, Feb. 1997.

[14] D. P. Chassin, Z. Huang, M. K. Donnelly, C. Hassler, E. Ramirez, and C. Ray, "Estimation of WECC system inertia using observed frequency transients," *IEEE Trans. Power Syst.*, vol. 20, no. 2, pt. 1, pp. 1190–1192, Apr. 2005.

[15] P. M Ashton, G. A. Taylor, A. M. Carter, M. E. Bradley, and W. Hung, "Application of phasor measurement units to estimate power system inertial frequency response," in *Proc. IEEE Power Energy Soc. Gen. Meeting*, Jul. 21–25, 2013, pp. 1–5.

[16] P. Wall, F. González-Longatt, and V. Terzija, "Estimation of generator inertia available during a disturbance," presented at the IEEE Power Energy Soc. Gen. Meeting, San Diego, CA, USA, 2012.

[17] T. Shu-Jen, L. Zhang, A. G. Phadke, Y. Liu, M. R. Ingram, S. C. Bell, I. S. Grant, D. T. Bradshaw, D. Lubkeman, and L. Tang, "Frequency sensitivity and electromechanical propagation simulation study in large power systems," *IEEE Trans. Circuits Syst. I, Reg. Papers*, vol. 54, no. 8, pp. 1819, 1828, Aug. 2007.

[18] P. M. Anderson and A. A. Fouad, *Power System Control and Stability*, 2nd ed. Piscataway, NJ, USA: IEEE, 2003.

[19] P. M. Anderson and M. Mirheydar, "A low-order system frequency response model," *IEEE Trans. Power Syst.*, vol. 5, no. 3, pp. 720–729, Aug. 1990.

[20] V. Terzija, "Improved recursive Newton-type algorithm for frequency and spectra estimation in power systems," *IEEE Trans. Instrum. Meas.*, vol. 52, no. 5, pp. 1654–1659, Oct. 2003.

Peter Wall received the B.Sc. degree in electrical and electronic engineering, the M.Sc. degree in power systems, and the Ph.D. degree in power systems from the University of Manchester, Manchester, U.K., in 2008, 2009, and 2013, respectively.

His main interests are power system dynamics, frequency stability, and intelligent controlled islanding. Currently, he is a Postdoctoral Research Associate at The University of Manchester.

Vladimir Terzija (M'95–SM'00) is the EPSRC Chair Professor in Power System Engineering, School of Electrical and Electronic Engineering, The University of Manchester, Manchester, U.K., where he has been since 2006. From 1997 to 1999, he was an Assistant Professor at the University of Belgrade. From 2000 to 2006, he was with ABB AG, Ratingen, Germany, working as an expert for switchgear and distribution automation.

His main research interests are the application of intelligent methods to power system monitoring, control, and protection, switchgear and fast transient processes, as well as digital-signal-processing applications in power.

Prof. Terziija received the Humboldt Research Fellowship in 1999.